An optimized protocol for iDISCO+ rat brain clearing, imaging, and analysis

Audrey Branch[1], Daniel Tward[1,3], Joshua T Vogelstein[3], Zhuhao Wu[4,5], and Michela Gallagher[2]

[1] Co-First authors

[2] Department of Psychological and Brain Sciences, Johns Hopkins University, Baltimore, USA.

[3] Department of Biomedical Engineering Johns Hopkins University Baltimore, USA.

[4] Department of Cell, Developmental & Regenerative Biology,

[5] Department of Neuroscience, Icahn School of Medicine at Mount Sinai, New York, USA.

Corresponding Author:

Audrey Branch, PhD

Department of Psychological and Brain Sciences

The Johns Hopkins University

3400 North Charles Street

116 Dunning Hall

Baltimore, MD 21218

Phone: 706-507-8770

Email: abranch@jhu.edu

Abstract

The advent of whole brain clearing and imaging methods have extended the breadth and depth at which neural populations can be studied. However, these methods have yet to be applied to larger brains, such as the brains of the common laboratory rat, despite the importance of these models in behavioral neuroscience research. Here we introduce an optimized iDISCO+ based immunolabeling and clearing methodology for application to adult rat brain hemispheres. We validate this methodology through the testing of common antibodies. In order to extend the accessibility of this methodology for general use, we have developed an open source platform for the registration of rat brain volumes to standard brain atlases for high throughput analysis.

Introduction

Understanding the structure and function of the myriad of cells comprising the central nervous system requires precise methods for labeling and measuring intact neural cell populations. The development of brain clearing protocols in recent years has greatly enhanced our ability to visualize fluorescently tagged cell populations in the intact brain. Such methods have now been used to identify components of coactivated neural populations using immediate early genes (Renier, Adams et al. 2016), to delineate connectivity between brain regions (Ye, Allen et al. 2016), to assess three-dimensional transcriptional profiling (Wang, Allen et al. 2018), to demonstrate complex connections between the nervous system and peripheral tissues (Chi, Wu et al. 2018, Wang, Allen et al. 2018), and to illuminate circuit level connectivity (Lerner, Shilyansky et al. 2015). However, these methods have yet to be applied broadly outside of the context of transgenic mouse models, as they are optimized to detect endogenous fluorescent reporters and are difficult to scale up for larger tissues. For example, while clearing methods have been tested for laboratory rat brains (Stefaniuk, Gualda et al. 2016), such applications often rely on the expression of fluorescent reporters. Rats have long been the model of choice for behavioral and cognitive neuroscience as they exhibit a broad and rich repertoire of quantifiable behaviors and their larger size assists in stereotaxic targeting of brain regions of interest. However, their larger size also presents a challenge in the application of brain clearing methodology, as these methods depend on the removal of lipids to achieve transparency. Furthermore, there is a relative deficit of transgenic rat models, limiting the potential application of clearing methods such CLARITY and CUBIC (Chung, Wallace et al. 2013, Susaki, Tainaka et al. 2015). Efforts to apply whole brain lightsheet imaging methods to rats models are further hampered by a deficit of data processing methods applicable to cleared rat brain tissue. Here we address these issues by outlining a brain clearing method that is optimized for application to rat brain hemispheres, and an open source platform optimized for registering the resulting lighsheet imaged brain data sets to a standard rat brain atlas.

Here, we successfully applied the iDISCO+ protocol to rat brain hemisphere. This protocol was chosen for its compatibility with immunolabeling, its simplicity, and its low cost. We first optimized the protocol to ensure even clearing throughout an intact rat brain hemisphere, and then applied it with immunolabeling against endogenous proteins and virally expressed reporters. To maximize the application of this method for use in rat models, we developed a registration method that can address lightsheet imaging artifacts simultaneously with alignment of the image set to any MRI based rat brain atlas, which can be run using a regular desktop computer.

Results

iDISCO+ delipidation and clearing for rat brain tissue

Rat brain tissue presents a challenge for whole brain clearing and imaging methodologies. The rat brain is larger than that of the mouse and contains a slightly different lipid and myelination profile. For optimal application to rat brain tissue, we reasoned that the protocol must be able to label endogenous or exogenous markers, as rat-based studies tend to rely on virally expressed or immunolabeled targets rather than endogenously expressed fluorescent markers. We began with the published iDISCO+ protocol (Renier, Adams et al. 2016) which is optimized for immunolabeling, using the suggested steps outlined for whole mouse brains. Initial application of this protocol to adult rat brain tissue (6 months) resulted in incomplete clearing in the center of the tissue and slight discoloration, likely due to incomplete removal of lipids and oxidation, respectively (Fig. 1B). Given the larger size and older chronological age of our rat subjects relative to the mice for which the protocol was developed (Fig.1D for size comparison) we speculated that rat brain tissue may require enhanced delipidation to fully clear the tissue, and thus sought to enhance the effectiveness of the lipid removal steps.

Toward this goal, we adapted the delipidation methods of the AdipoClear protocol (Chi, Wu et al. 2018), which was developed to clear and immunolabel lipid dense adipose tissue without damaging tissue structure. A schematic of this modified protocol with relevant additions and substitutions is shown in Fig.1A, alongside rat brain hemisphere cleared with this new protocol (Fig1C), as compared to results of the previous version of the protocol (Fig1B). A full outline of protocol steps and recommendations can be found in Supplemental Figure 1.

In order to ensure that the modification of the protocol did not interfere with immunolabeling, we tested several different antibodies which have previously been shown to be compatible with iDISCO+. Brains were imaged using a LaVision BioTec Ultramicroscope with a 2X variable zoom lens, which allows for an entire rat brain hemisphere to be imaged in either sagittal or horizontal orientation. To achieve even illumination across the tissue, both lasers were used for all scans and the maximum lightsheet width and NA were used. The measured z resolution (thickness) of the lightsheet with this configuration is ~2.5 µm at its thinnest point (LaVision BioTec's information). Figure 2 shows representative results of staining in a rat brain with several common antibodies. Images are shown for anti-tyrosine hydroxylase staining throughout the z-extent of the tissue, demonstrating no loss of image resolution with increasing z-depth (Fig. 1 A-K). Previously validated antibodies including parvalbumin (Fig2L), cFos (Fig.2M) and GFP and RFP (Fig.2N) are also compatible with the protocol.

Registration of cleared brain image data to rat brain atlas

Extracting meaningful information from cleared intact brain tissue typically involves quantifying the distribution of labeled celled cells within anatomically meaningful regions. Our imaging of rat brain hemispheres generated data sets with ~2500 tiffs per channel in sagittal orientation and ~3500 in horizontal and are therefore too large to be manually annotated. While some methods do exist for automatically register lightsheet imaged brains to atlases, they are typically designed for use with mouse tissue (Renier, Adams et al. 2016) or for application to aqueous based clearing methods (Susaki, Tainaka et al. 2015, Kutten 2016), which have a very different intensity profile than tissue cleared with iDISCO. We therefore sought to develop an automated annotation method optimized for iDISCO+

cleared rat brain tissue. The most common approach to this form of annotation involves estimating a nonlinear registration between observed data and a well characterized atlas, then using the transformation to transfer annotations from the atlas onto the observed dataset. A variety of methods exist for registering medical image data to standard brain atlases (Klein, Andersson et al. 2009). Given the similarity of the data structure between MRI and cleared brain imaging, efforts have been made to apply these methods for the registration of cleared brain image sets to atlases, using a combination of rigid and or affine deformations of the sample data to align it with the atlas space (Susaki, Tainaka et al. 2015, Renier, Adams et al. 2016).

However, light sheet microscopy images of cleared tissue present challenges not seen in human MRI. Specifically, the major challenges needing to be addressed are image registration in the presence of missing or damaged tissue and variable image contrast. We use an image registration framework developed originally for digital pathology (Tward 2019) that functions robustly in the presence of these issues. In this framework, contrast differences between atlas images and target images are estimated jointly with image registration parameters. The location of missing and damaged tissue or other artifacts, is also estimated jointly in an iterative fashion using the Expectation Maximization algorithm (Dempster 1977).

Our starting data set was obtained by imaging a rat brain hemisphere positioned in sagittal orientation using a 2X variable zoom objective at a 0.63X zoom setting (1.2X effective magnification). Using the 488nm laser and imaging from through the z extent of the hemisphere with a 2.5 um step size resulted in a data set of 2500 individual tiffs representing autofluorescent intensity profile of major anatomical structures throughout the entirety of the hemisphere. We choose the Waxholm MRI atlas (Papp, Leergaard et al. 2014, Kjonigsen, Lillehaug et al. 2015) for initial testing of the alignment of this data set with this methodology. An example result illustrating image annotation through registration is shown in Fig. 4. Panel C shows anatomical structures defined in the atlas as colors, overlayed on the the grayscale atlas image. A good alignment can readily be observed for subcortical gray matter structures, as well as for cortical boundaries. Panel D shows a comparison between atlas and target image intensities, where yellow indicates relatively good agreement between the images.

Image registration typically involves many parameter choices that result in a barrier to use for neuroscientists. Our approach to improving accessibility is to make several examples publicly available through github [https://github.com/dtward/image_lddmm_tensorflow], using Jupyter notebooks [https://jupyter.org/] as an intuitive web browser based interface. See Example_iDISCO_rat_waxholm.ipynb in the repository for one example from which the figures in this paper are generated. All necessary parameter choices have been made and justified within the Jupyter notebook. This approach can be extended to a variety of other model organisms and humans and will be the subject of future work.

Discussion

Unbiased assessment of neuronal populations in intact brains is a valuable exploratory tool, but remains limited in its application. We have developed a brain clearing methodology that is capable of evenly immunolabeling and clearing an adult rat brain hemisphere using adult Long Evans rats. We began by applying the solvent based iDISCO+ (Renier, Adams et al. 2016) methodology, which offers several advantages for application to the larger brain of the common Long Evans outbred rat strain. iDISCO+

delipidation and clearing causes minimal distortion of tissue size as compared to aqueous based protocols which tend to enlarge samples (Wan, Zhu et al. 2018) and was developed to optimize the penetration of antibodies for immunolabeling of endogenous proteins. In addition, the inherent autofluorescence present in the 488nm wavelength spectrum of iDISCO+ cleared brains provides highly detailed structural information which can be used to register resulting image data sets to standard MRI based brain atlases. Taken together, this brain clearing and imaging platform makes efficient analysis of cleared rat brains attainable for use in the common laboratory rat.

Methods

Animals

Young male Long-Evans rats were obtained at 4-6 months of age from Charles River Laboratories (Raleigh, NC) and housed in a vivarium at Johns Hopkins University until 24-26 months of age. All rats were individually housed at 25°C and maintained on a 12 hr light/dark cycle. Food and water were provided ad libitum until indicated otherwise. The rats were examined for health and pathogen-free status throughout the study, as well as necropsies at the time of sacrifice. All procedures were approved by the Johns Hopkins University Institutional Animal Care and Use Committee in accordance with the National Institutes of Health directive.

Sample collection

Young adult male rats (6-10 months old) were heavily anesthetized with an overdose of isofluorane and intracardiac perfusion and fixation was performed with PBS+NaN3 followed by 4% PFA. All samples were post-fixed in 4% PFA at 4°C overnight. Fixed samples were then washed in PBS+NaN3 for 1 hour three times.

iDISCO+ Rat Protocol

Reagent	Reference
PBS 10X	Ambion AM9624
ParaFormAldehyde 16% (PFA)	EMS 15710-S
Triton X-100	Sigma X100-500ML
Tween-20	Sigma P9416-100ML
Glycine	Sigma G7126-500G
Sodium Azide (NaN3)	58032-100G
10N Sodium Hydroxide (NaOH)	Fisher SS255-1

Heparin	Sigma H3393-50KU
DMSO	Fisher D128-4
Methanol (MeOH)	Fisher A412SK-4
Hydrogen Peroxide 30% (H2O2)	Sigma 216763-100ML
DiChloroMethane (DCM)	Sigma 270997-12X100ML
DiBenzylEther (DBE)	Sigma 108014-1KG or 3KG
methyl-β-cyclodextrin (MβCD)	Sigma 332615
2-Mercaptoethanol (βME)	Sigma M6250

Delipidation and Permeabilization

Fixed samples were washed in B1n buffer 2 hr, 4 hr, and overnight. Samples were then washed/dehydrated in a 20%, 40%, 60%, 80% MeOH/B1n gradient for 1 hr each. Samples were then treated with 100% dichloromethane (DCM) for 30 minutes three times, then overnight. DCM was washed out with 100% MeOH for 1.5 hr, 3 hr, and overnight and rehydrated with a reverse gradient of MeOH/B1n 80%, 60%, 40%, 20% for 1 hr each, and 100% B1n for 1hr then overnight. This was followed by washes with SdC buffer for 4 hr followed by 2 x 24 hrs, and 2 x 48 hrs. Finally, samples were treated with a 5% DMSO/0.3M Glycine/PTxwH solution at 37°C for 6h and overnight, then washed in PTwH for 1.5 hr, 3 hr, and overnight. All steps were performed with shaking at 150 RPM.

Immunolabeling

Samples were incubated in primary antibody solution (primary antibody, DMSO, glycine, PTwH) for 8 days. After primary antibody incubation, samples were washed in PTwH for 3hr, 4hr, overnight, and 4 x 24hrs to wash out residual primary antibody. Samples were then incubated for 8 days in secondary antibody solution (secondary antibody, PTwH), then washed PTwH for 3hr, 4hr, overnight, and 4 x 24hrs to wash out residual secondary antibody. In this study, we tested the following primary antibodies: rabbit anti-cFos (Cell Signaling, cat# 2250 ; 1:200), rabbit anti-parvalbumin (Swant, cat#: PV27, 1:200), sheep anti-tyrosine hydroxylase (Millipore, AB1542, 1:200), chicken anti-GFP (Aves, cat#: GFP-1020, 1:1000), and rabbit anti-RFP (Rockland, cat.#: 600-401-379, 1:1000). Secondary antibodies were used at the same concentration as their respective primary antibodies and included donkey anti-rabbit 568 (ThermoFisher, cat# A10042), donkey anti-chicken 647 (Millipore, cat# AP194SA6) or donkey anti-sheep 647 (ThermoFisher, cat# A-21448).

Tissue Clearing

Samples were post-fixed in 2% PFA overnight at 4°C, then dehydrated in 20%, 40%, 60%, 80%, 100% H2O/MeOH series for 30 minutes at each step at RT. Following dehydration, samples were washed with 100% DCM 2 x 1.5hr, 3hr, and overnight, followed by clearing with DBE. Samples were stored in the dark until imaging.

Lightsheet imaging

All samples were imaged on a lightsheet microscope (Ultramicroscope II, LaVision Biotec) equipped with a 2X (low magnification, whole brain) or 4X (high magnification) lens and a sCMOs camera (Andor Neo). Images were acquired with the ImspectorPro software (LaVision BioTec). For imaging, samples were clamped in place to the sample holder in sagittal orientation (midline up), or horizontal orientation (dorsal up) and placed in an imaging reservoir filled with DBE and illuminated from the side by the laser light sheet. The samples were scanned with the 488 (filter: 575/40 , 561 (filter: 620/60), and 640nm (filter: 680/30) laser channels with a step size of 2.5 µm for the 2X objective on 0.6X zoom setting (1.2X effective magnification), resulting 3D image sets with approximately 2.5 μm^3 voxel size.

Image processing

Several preprocessing steps were used before registration. First, streak correction was performed by zeroing out signal at -10.5 degrees, 0 degrees, and 10 degrees in the Fourier domain as shown in Figure 3. These artifacts are associated to shadowing when tissue boundaries are parallel to the light source. Second, slice to slice intensity variations were corrected such that the mean signal changed smoothly across slices. To accomplish this, mean intensity was computed as a function of slice number, and the resulting signal was smoothed using a Gaussian kernel with standard deviation 33 slices. Each slice intensity was then normalized by dividing by its mean intensity, and multiplied by its smoothed intensity. Third, 3D images were inhomogeneity corrected using the N4 algorithm implemented in simple ITK (Tustison, Avants et al. 2010). Fourth, images were downsampled by averaging neighboring voxels, to a resolution of 0.077 mm. This corresponds approximately to the resolution of the Waxholm MRI atlas after a factor of 2 downsampling.

Images for figures were generated using ImageJ. For signal channels, background subtraction was performed using a 50 um rolling ball radius. For figures showing autofluorescent channels, no image modification was performed other than those discussed in each figure.

Registration

We perform deformable image registration between the autofluorescence channel $J : X \subset R^3 \rightarrow R$ (this notation means "J is a function that maps points in some subset of 3D space to real numbers") and the Waxholm T2* rat atlas $I : X \rightarrow R$. Autofluorescence has been successfully used for registration in similar modalities such as CLARITY (Kutten 2016).

We construct spatial transformations $\phi : X \rightarrow X$ using the Large Deformation Diffeomorphic Metric Mapping model (Beg M.F 2005) solving a variational problem to minimize the weighted sum of a regularization cost and a matching cost. The diffeomorphic property (smooth, 1 to 1, with smooth inverse) is ensured by defining ϕ as the flow of a smooth velocity field $v_t : X \rightarrow R^3$ for $t \in [0,1]$:

$$\varphi(x) = x + \int_0^1 v_t(\varphi_t(x))dt$$

Sufficient smoothness is ensured by defining a regularization function via

$$R(v) = \frac{1}{2\sigma_R^2} \int_0^1 \int_X |Lv_t(x)|^2 dxdt \ ,$$

where L is the differential operator $L = (id - a^2\Delta)^p$ (Dupuis P. 1998) for a a smoothness scale (with units of length), Δ the Laplacian ($\frac{\partial^2}{\partial x^2} + \frac{\partial^2}{\partial y^2} + \frac{\partial^2}{\partial z^2}$), and $p \geq 2$ power. We choose a =2 voxels (double check!) and p = 2. The parameter σ_R^2 is a weighting factor.

To choose an appropriate matching cost, we must overcome several important challenges intrinsic to this data. The image intensity profile differs from the MRI atlas, and tissue is missing due to cutting and limited field of view, artifacts are present.

We overcome these challenges simultaneously using estimation within a generative statistical model, rather than proposing a series of steps in a pipeline. Instead of using a similarity function such as normalized cross correlation or mutual information, we predict J in terms of $\tilde{I} =: I(\phi^{-1})$ and use a simple Gaussian white noise model as a cost (sum of square error).

$$M(\tilde{I}) = \frac{1}{2\sigma_M^2} \int |F_\theta(\tilde{I}(x)) - J(x)|^2 dx$$

Where $F_c(t) = \sum_{i=0}^{3} c_i t^i$ is a cubic polynomial which predicts the intensities in J from those in $\tilde{I}$. The factor σ_M^2 is a weighting factor, chosen to be approximately equal to the variance of the noise in our Gaussian white noise model.

Using a white noise model allows us to accommodate missing data using the expectation maximization algorithm, as discussed in (Tward 2019). In each E step we compute posterior probabilities that tissue falls into one of two classes: some location in the atlas image ((M)atching), or (A)rtifact and missing tissue. The data likelihood under the first class uses the model described above, while the latter is thought of as constant intensity (unknown mean c_A) with Gaussian white noise of variance σ_A^2. We choose $\sigma_A^2 = 10\sigma_M^2$. Let $f_i(x) = \frac{1}{\sqrt{2\pi\sigma_i^2}} \exp\left(-x^2/2\sigma_i^2\right),\ i \in \{M, A\}$ be a zero mean Gaussian CDF, the posteriors for the first class is

$$p(x) = \frac{f_M(F_\theta(\tilde{I}(x)) - J(x))}{f_M(F_\theta(\tilde{I}(x)) - J(x)) + f_A(c_A - J(x))}.$$

In the M step each unknown parameter is estimated by minimizing our cost function weighted by the posterior above. The mean c_A can be found exactly via a weighted average. The ϑ can be found exactly by solving a linear equation (weighted least squares). In both cases the weights at each voxel are given by p(x). The v_t is estimated iteratively using weighted LDDMM, as described in (Tward 2019).

EM iterations result in a monotonically increasing complete data likelihood (Dempster 1977). We note that this approach to missing data is only possible because our cost function represents a negative log likelihood.

This procedure was implemented in python tensorflow [https://www.tensorflow.org/], handling high performance computing requirements such as parallelizing across multiple cores or GPU.

Working examples are prepared through jupyter notebooks jupyter.org and made publicly available through neurodata.io/ndreg.

Registration Interface

An example Jupyter notebook illustrating our registration procedure can be found here: https://github.com/neurodata/ndreg and a walkthrough can be found in Supplemental Materials. The registration procedure includes preprocessing, followed by registration at 2 different resolutions, using the lower resolution result as an initial guess for unknown parameters at higher resolution. The following figures shows an overview of the notebook, with user inputs, atlas processing, atlas orientation verification, tif processing, target orientation verification, and registration error at low and high resolution. Users can download this notebook and simply replace filenames with their data.

Funding sources:

We would like to acknowledge generous support from the National Institute of Health (NIH) (grant P01AG009973 "Cognitive and Hippocampal/Cortical Systems in Aging" to MG), the National Science Foundation (NSF) (Award Number EEC-1707298 to JTV), and the Johns Hopkins University Kavli Neuroscience Discovery Institute Postdoctoral Fellowship to AB and DT.

References

Beg M.F, M. M. I., Trouve A., Younes L. (2005). "Computing large deformation metric mappings via geodesic flows of diffeomorphisms. ." International Journal of Computer Vision **61**(2): 139-157.

Chi, J., Z. Wu, C. H. J. Choi, L. Nguyen, S. Tegegne, S. E. Ackerman, A. Crane, F. Marchildon, M. Tessier-Lavigne and P. Cohen (2018). "Three-Dimensional Adipose Tissue Imaging Reveals Regional Variation in Beige Fat Biogenesis and PRDM16-Dependent Sympathetic Neurite Density." Cell Metab **27**(1): 226-236 e223.

Chung, K., J. Wallace, S. Y. Kim, S. Kalyanasundaram, A. S. Andalman, T. J. Davidson, J. J. Mirzabekov, K. A. Zalocusky, J. Mattis, A. K. Denisin, S. Pak, H. Bernstein, C. Ramakrishnan, L. Grosenick, V. Gradinaru and K. Deisseroth (2013). "Structural and molecular interrogation of intact biological systems." Nature **497**(7449): 332-337.

Dempster, A. P., Laird, N.M. and Rubin, D.B. (1977). "Maximum likelihood from incomplete data via the EM algorithm." Journal of the Royal Statistical Society: Series B (Methodological) **39**(1): 1-22.

Dupuis P., G. U., Miller M.I. (1998). "Variational problems on flows of diffeomorphisms for image matching." Quarterly of Applied Mathematics. **LVI**(3): 587-600.

Kjonigsen, L. J., S. Lillehaug, J. G. Bjaalie, M. P. Witter and T. B. Leergaard (2015). "Waxholm Space atlas of the rat brain hippocampal region: three-dimensional delineations based on magnetic resonance and diffusion tensor imaging." Neuroimage **108**: 441-449.

Klein, A., J. Andersson, B. A. Ardekani, J. Ashburner, B. Avants, M. C. Chiang, G. E. Christensen, D. L. Collins, J. Gee, P. Hellier, J. H. Song, M. Jenkinson, C. Lepage, D. Rueckert, P. Thompson, T. Vercauteren, R. P. Woods, J. J. Mann and R. V. Parsey (2009). "Evaluation of 14 nonlinear deformation algorithms applied to human brain MRI registration." Neuroimage **46**(3): 786-802.

Kutten, K. S., Vogelstein, J.T., Charon, N., Ye, L., Deisseroth, K., Miller, M.I. (2016). "Deformably Registering and Annotating Whole CLARITY Brains to an Atlas via Masked LDDMM." Proc. SPIE 9896 Optics, Photonics and Digital Technologies for Imaging Applications IV **arXiv:1605.02060**
Lerner, T. N., C. Shilyansky, T. J. Davidson, K. E. Evans, K. T. Beier, K. A. Zalocusky, A. K. Crow, R. C. Malenka, L. Luo, R. Tomer and K. Deisseroth (2015). "Intact-Brain Analyses Reveal Distinct Information Carried by SNc Dopamine Subcircuits." Cell **162**(3): 635-647.
Papp, E. A., T. B. Leergaard, E. Calabrese, G. A. Johnson and J. G. Bjaalie (2014). "Waxholm Space atlas of the Sprague Dawley rat brain." Neuroimage **97**: 374-386.
Renier, N., E. L. Adams, C. Kirst, Z. Wu, R. Azevedo, J. Kohl, A. E. Autry, L. Kadiri, K. Umadevi Venkataraju, Y. Zhou, V. X. Wang, C. Y. Tang, O. Olsen, C. Dulac, P. Osten and M. Tessier-Lavigne (2016). "Mapping of Brain Activity by Automated Volume Analysis of Immediate Early Genes." Cell **165**(7): 1789-1802.
Stefaniuk, M., E. J. Gualda, M. Pawlowska, D. Legutko, P. Matryba, P. Koza, W. Konopka, D. Owczarek, M. Wawrzyniak, P. Loza-Alvarez and L. Kaczmarek (2016). "Light-sheet microscopy imaging of a whole cleared rat brain with Thy1-GFP transgene." Sci Rep **6**: 28209.
Susaki, E. A., K. Tainaka, D. Perrin, H. Yukinaga, A. Kuno and H. R. Ueda (2015). "Advanced CUBIC protocols for whole-brain and whole-body clearing and imaging." Nat Protoc **10**(11): 1709-1727.
Tustison, N. J., B. B. Avants, P. A. Cook, Y. Zheng, A. Egan, P. A. Yushkevich and J. C. Gee (2010). "N4ITK: improved N3 bias correction." IEEE Trans Med Imaging **29**(6): 1310-1320.
Tward, D. J., Brown, T., Kageyama, Y., Patel, J., Hou, Z., Mori, S., Albert, M., Troncoso, J. and Miller, M. (2019). "Diffeomorphic registration with intensity transformation and missing data: Application to 3D digital pathology of Alzheimer's disease." BioRxiv.
Wan, P., J. Zhu, J. Xu, Y. Li, T. Yu and D. Zhu (2018). "Evaluation of seven optical clearing methods in mouse brain." Neurophotonics **5**(3): 035007.
Wang, X., W. E. Allen, M. A. Wright, E. L. Sylwestrak, N. Samusik, S. Vesuna, K. Evans, C. Liu, C. Ramakrishnan, J. Liu, G. P. Nolan, F. A. Bava and K. Deisseroth (2018). "Three-dimensional intact-tissue sequencing of single-cell transcriptional states." Science **361**(6400).
Ye, L., W. E. Allen, K. R. Thompson, Q. Tian, B. Hsueh, C. Ramakrishnan, A. C. Wang, J. H. Jennings, A. Adhikari, C. H. Halpern, I. B. Witten, A. L. Barth, L. Luo, J. A. McNab and K. Deisseroth (2016). "Wiring and Molecular Features of Prefrontal Ensembles Representing Distinct Experiences." Cell **165**(7): 1776-1788.

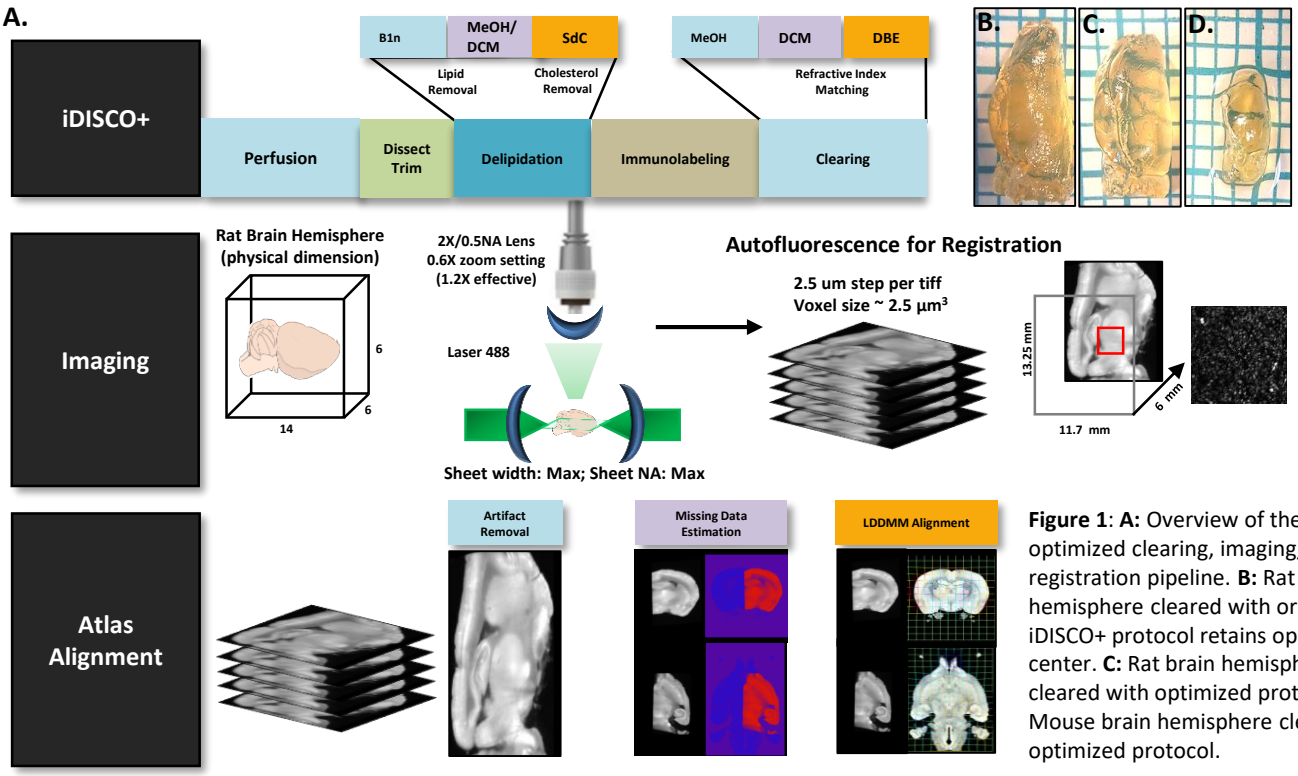

Figure 1: **A:** Overview of the rat brain optimized clearing, imaging, and registration pipeline. **B:** Rat brain hemisphere cleared with original iDISCO+ protocol retains opaque center. **C:** Rat brain hemisphere cleared with optimized protocol. **D:** Mouse brain hemisphere cleared with optimized protocol.

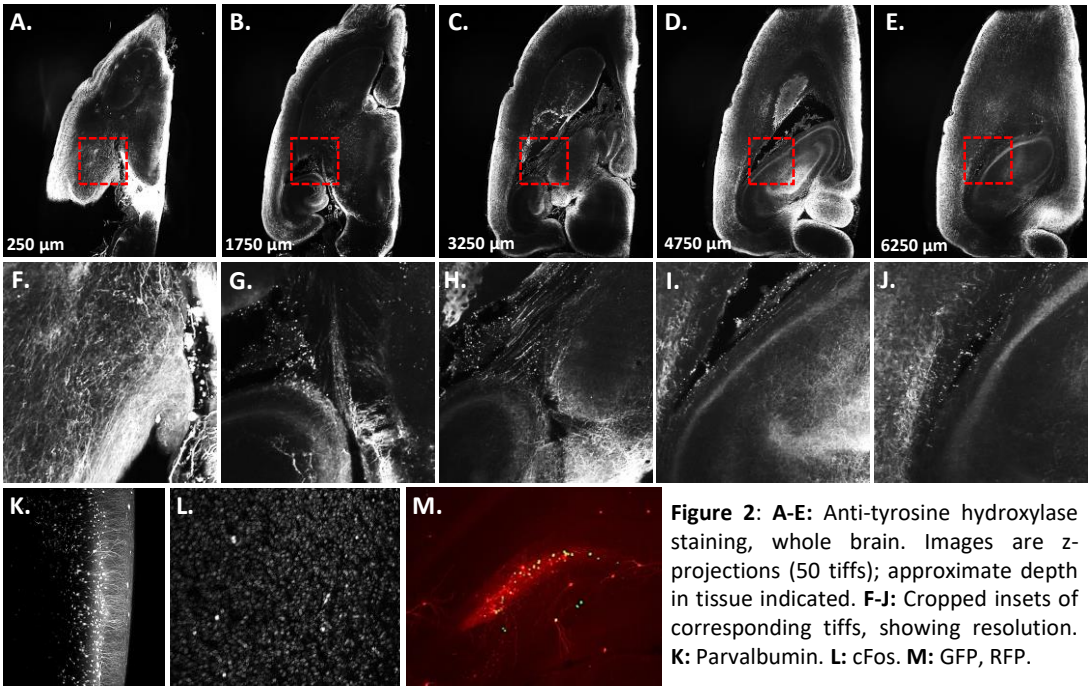

Figure 2: **A-E:** Anti-tyrosine hydroxylase staining, whole brain. Images are z-projections (50 tiffs); approximate depth in tissue indicated. **F-J:** Cropped insets of corresponding tiffs, showing resolution. **K:** Parvalbumin. **L:** cFos. **M:** GFP, RFP.

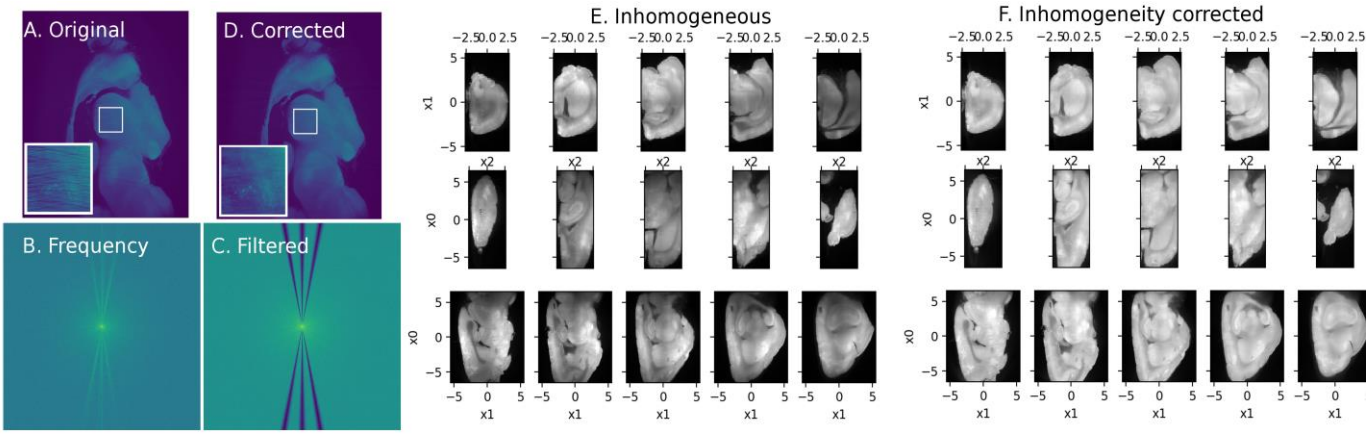

Figure 3: Imaging artifact correction. **A-D**: Streak correction. Left: before filtering, right: after filtering. Top: spatial domain, bottom: frequency domain. **E, F:** Nonuniformity correction. Nonuniform image (**E**) is corrected (**F**) using a spatially smooth multiplicative transform. Axes x0, x1, and x2 have units in mm.

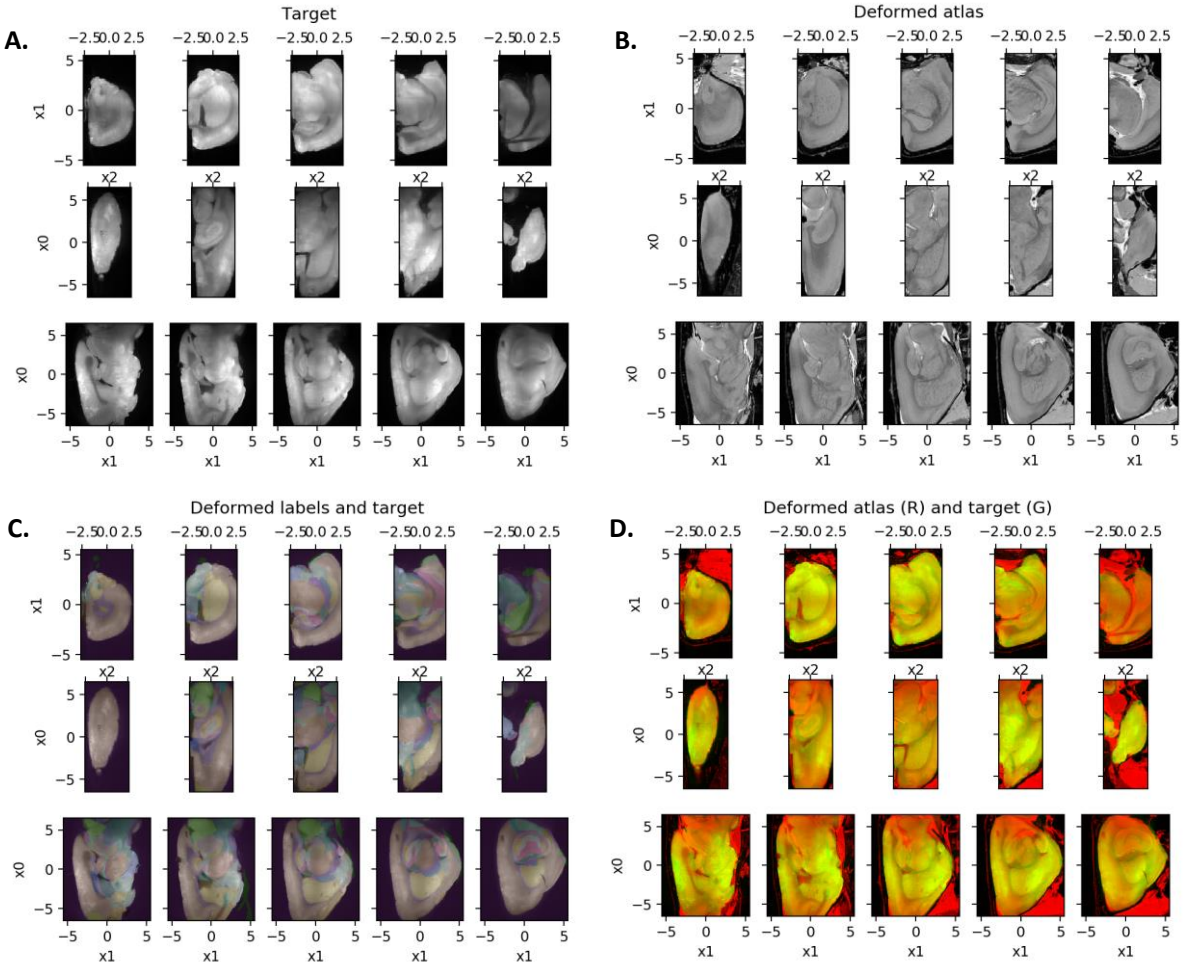

Figure 4 . **A:** Target image is aligned with a deformed atlas image (**B**). Annotation labels are showed overlaid on target image (**C**), and both images are shown as red and green channels (**D**) yielding yellow where image intensities are similar. All images are shown with 5 slices in 3 planes.